NASA-CR-202669

ASTROPHYSICAL ADAPTATION OF POINTS, THE PRECISION OPTICAL INTERFEROMETER IN SPACE

GRANT NO. NAGW-4768

Final Report

For the Period 1 July 1995 through 30 June 1996

Principal Investigator

Dr. Robert D. Reasenberg

October 1996

Prepared for

National Aeronautics and Space Administration
Washington, D.C.

Smithsonian Institution
Astrophysical Observatory
Cambridge, Massachusetts 02138

The Smithsonian Astrophysical Observatory
is a member of the
Harvard-Smithsonian Center for
Astrophysics

The NASA Technical Officer for this grant is Michael Kaplan, Code SZH.

POINTS: high astrometric capacity at modest cost *via* focused design

Robert D. Reasenberg, Robert W. Babcock, Marc A. Murison*,
M. Charles Noecker*, and James D. Phillips
Smithsonian Astrophysical Observatory
Harvard-Smithsonian Center for Astrophysics, Cambridge, MA 02138

Bonny L. Schumaker and James S. Ulvestad
Jet Propulsion Laboratory
California Institute of Technology, Pasadena, CA 91109

William McKinley* and Robert J. Zielinski*
Itek Optical Systems, Lexington, MA 02173

Charles F. Lillie
TRW, Redondo Beach, CA 90278

ABSTRACT

POINTS (Precision Optical INTerferometer in Space) would perform microarcsecond optical astrometric measurements from space, yielding submicroarcsecond astrometric results from the mission. It comprises a pair of independent Michelson stellar interferometers and a laser metrology system that measures both the critical starlight paths and the angle between the baselines. The instrument has two baselines of 2 m, each with two subapertures of 35 cm; by articulating the angle between the baselines, it observes targets separated by 87 to 93 deg. POINTS does global astrometry, i.e., it measures widely separated targets, which yields closure calibration, numerous bright reference stars, and absolute parallax. Simplicity, stability, and the mitigation of systematic error are the central design themes. The instrument has only three moving-part mechanisms, and only one of these must move with sub-milliradian precision; the other two can tolerate a precision of several tenths of a degree. Optical surfaces preceding the beamsplitter or its fold flat are interferometrically critical; on each side of the interferometer, there are only three such. Thus, light loss and wavefront distortion are minimized.

POINTS represents a minimalistic design developed *ab initio* for space. Since it is intended for astrometry, and therefore does not require the u-v-plane coverage of an imaging instrument, each interferometer need have only two subapertures. The design relies on articulation of the angle between the interferometers and body pointing to select targets; the observations are restricted to the "instrument plane." That plane, which is fixed in the pointed instrument, is defined by the sensitive direction for the two interferometers. Thus, there is no need for siderostats and moving delay lines, which would have added many precision mechanisms with rolling and sliding parts that would be required to function throughout the mission. Further, there is no need for a third interferometer, as is required when out-of-plane observations are made.

An instrument for astrometry, unlike those for imaging, can be compact and yet scientifically productive. The POINTS instrument is compact and therefore requires no deployment of precision structures, has no low-frequency (i.e., under 100 Hz) vibration modes, and is relatively easy to control thermally. Because of its small size and mass, it is easily and quickly repointed between observations. Further, because of the low mass, it can be economically launched into high Earth orbit which, in conjunction with a solar shield, yields nearly unrestricted sky coverage and a stable thermal environment.

Keywords: astrometry, interferometry, metrology, spacecraft

---

* Present Addresses: M.A. Murison, U.S Naval Observatory; M.C. Noecker, Ball Aerospace and Technologies Corp.; W. McKinley, Hughes Danbury Optical Systems; R.J. Zielinski, Adaptive Optics Associates, Inc.

Final report under NASA grant NAGW-4768 in response to SAO proposal P3377-12-94 for the Astrophysical Adaptation of POINTS, the Precision Optical INTerferometer in Space.

The proposal, in response to the New Missions Concepts NRA (94-OSS-15), called for two-year funding of $235,420; the funding provided was $49,993. The revised work statement selected from the original tasks and noted that, at the reduced level of funding, the analyses would not be carried out as deeply as originally planned. Funding was later augmented by $40,000 in response to SAO proposal P3683-2-96 "to prepare for and participate in a NASA review of Orbiting Stellar Interferometer (OSI) and POINTS." Technical work done under both the initial funding and the augmentation was incorporated into the SAO report dated 4 March 1996 and submitted to NASA for the OSI-POINTS review. Some additional information was contained in the SAO-supplied handout in coordination with the presentation by the PI at the review at LPI on 26 March 1996. Finally, many of the results of the work were incorporated in *POINTS: High Astrometric Capacity at Modest Cost vis Focused Design*, Reasenberg et al., Proc. SPIE, vol. 2807, in press 1996, copy appended. This paper represents the state of the POINTS project at the end of NASA funding. (An additional paper on the detection with POINTS of remote planets is in preparation, but does not represent work under the subject grant.)

2. POINTS CHARACTERISTICS

2.1 Instrument description and concept

Mitigation of systematic error is the central theme of the POINTS architecture and data-analysis methods. The instrument uses stable materials, precise thermal control, and continuous precise metrology. The data-analysis provides post-measurement detection and correction of time-dependent bias. We demonstrated the required picometer (pm, 10^{-12} m) laser metrology for POINTS in November 1991,[1] and in May 1992 filed for a patent, which has now been issued.[2] Another method was demonstrated by the OSI team a year later.[3] Techniques applicable to aligning laser gauges were demonstrated by Sampas & Anderson[4] and are more than adequate for POINTS.

The principal elements of the POINTS instrument are two starlight interferometers, mounted at a relative angle (φ) that can be varied between 87° and 93°, a metrology system, and a fine-pointing system. Since φ will be adjustable between 87° and 93°, a reference star can be selected from a band that includes 5% of the sky. The adjustment of φ employs the only precision mechanism in the instrument. Table I lists the principal parameters of the POINTS instrument.

A single POINTS measurement determines θ, the angular separation of a pair of target stars. For a pair of mag 8 stars, POINTS reaches its nominal measurement accuracy of 2 μas (standard error) with about a 140 sec observation. An observation would be preceded by a slew and adjustment of φ requiring, on average, 75 seconds[5] and by an additional time to damp vibrations and acquire the targets, which is under 25 seconds. No additional time is required for set up, such as configuring the instrument based on the type of targets to be observed. In operation, the difficult problem of measuring the angular separation of two widely spaced stars is reduced to two less difficult problems: that of measuring φ, the angle between the two stellar interferometers, and that of measuring δ_1 and δ_2, the (subarcsec scale) offsets of the target stars from their respective interferometer axes.

In each of the two starlight interferometers, two afocal telescopes compress samples of the starlight, which are directed toward the beamsplitter and spectrometers. See Figure 1. At the exit ports of the beamsplitter, the light is dispersed and focused onto a pair of detector arrays. The patterns of interference on the arrays form the basis for estimating δ. This spectrometer allows the interferometers to function when the instrument is pointed several arcsec from the target. However, for high fringe visibility (and correspondingly high astrometric information rate), the pointing offset should be kept much smaller than δ_N, the Nyquist angle of 4.6 arcsec, at which the total number of fringes is half the number of detector pixels.

We first publicly discussed the dispersed-fringe approach in 1978,[6] long before it became popular. This approach has three advantages over a single-detector measurement of the white-light fringe. First, it preserves information on complex targets (e.g., a binary), allowing re-analysis of data from a target originally presumed to be simple. Second, it enables optimal use of photons near the intensity minima, as discussed in connection with Eq. (3). Finally, its expanded range of pointing offset simplifies initial fringe acquisition.

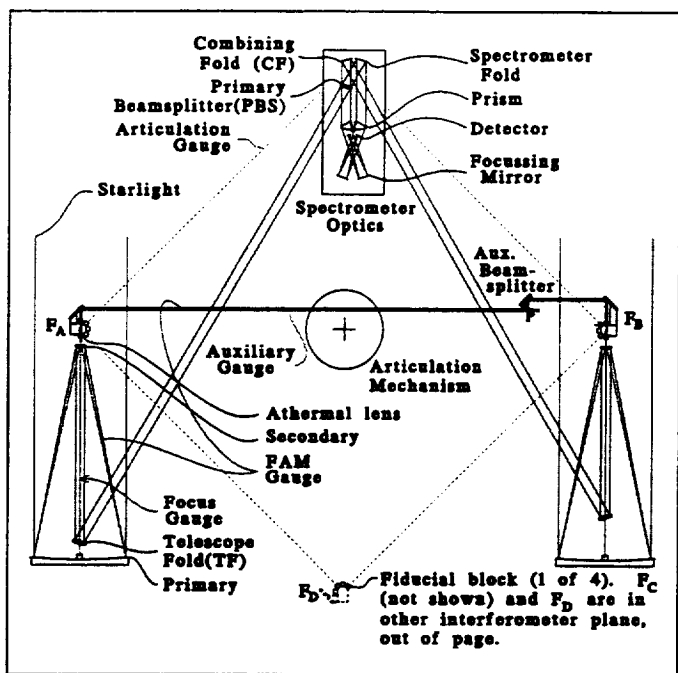| Table I. Principal parameters of the POINTS instrument	
Interferometer	
2	stellar interferometers
2 m	baseline length
87-93°	angle between baselines (adjustable)
2	subapertures per interferometer
35 cm	subaperture outer diameter
15 cm	diameter of central obscuration
0.25-0.9 μm	optical passband
15%	average photon detection probability
Spectrometer	
3.5 cm	beam size
29°	prism angle (material: fused silica)
17 cm	parabolic mirror focal length
3-7	fringes across the passband
256	pixels across the CCD
20 μm	pixel size
2.4 arcsec	pixel projected on sky
Measurement	
2 μas	single-measurement standard error
140 sec	observation time (two mag 8 stars)
9.5 mag	faint limit of "bright star"
14 mag	"faint star" limit without slit
18 mag	"faint star" limit with slit
21 mag	"faint star" limit with small insertable slit (not to full accuracy; adds a mechanism)

Figure 1. Single interferometer optical plan.

Figure 2 shows the optical bench for one stellar interferometer. It has a box-like structure of graphite-cyanate sheets. The cylindrical space near the center of the bench is for a pair of large flexure (articulation) pivots that join the two interferometers.[7] The angle between the two interferometers is changed by a linear drive that pushes between the benches at a radius of about 1 m, and is countered by a spring. The drive has a (1 mm pitch) roller screw turned by a (200 step/revolution) stepping motor with redundant windings for the large motion, and a (15-25 μm PMN or PZT) actuator stack for fine control. A coarse sensor (e.g., LVDT or Inductosyn) on the linear actuator would crudely determine φ and control the range of motion of the drive.

Pointing with arcsec precision is provided by the bus using Hubble-type reaction wheels, star trackers, and gyros. Within the instrument housing, there is a hexapod Fine Pointing and Isolation System (FPIS) that holds the instrument stable on the target; it uses a blended signal from instrument-mounted star trackers, the instrument *per se*, and accelerometers built into the hexapod's struts.

The high-precision star-position measurement of δ is made with respect to the optical axis of the interferometer. In turn, the position of this axis is a consequence of the positions of the optical elements used to transfer the starlight. The metrology system must measure, to about 1.3 pm overall accuracy, average changes in the starlight optical path difference (OPD) induced in each interferometer by all motions and distortions of all optical elements. Our approach is to use Full-Aperture Metrology (FAM), which we introduced into the design a dozen years ago.[8,9] The pm precision of the laser gauges is employed effectively in FAM by introducing laser light that illuminates the full starlight aperture. A small fraction of the laser light is diffracted at shallow zone plates on the primaries, and thereafter travels a path nearly identical to that of the starlight.[10] FAM provides three significant advantages over conventional approaches, which use laser gauges to measure between discrete endpoints, e.g., retroreflectors. (a) FAM is less complicated. (b) FAM measures more nearly the correct quantity. (c) FAM collects the effects on OPD of the positions of all starlight optics of one interferometer into the locations of a pair of *fiducial points*, which define the interferometer *pseudobaseline* and, in so doing, permits measurement of the angle between interferometers.
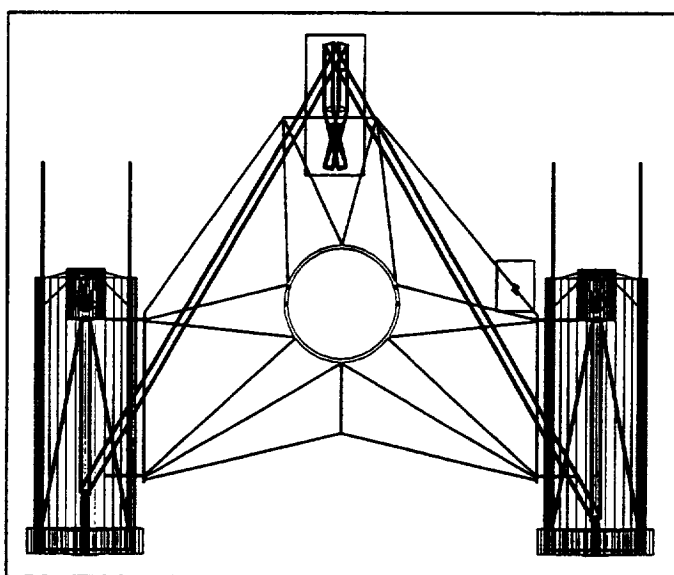
2.2 Observing

The wide separation between target stars makes POINTS a global astrometric instrument. For simplicity and efficiency, the set of observed objects is divided into reference-grid stars and other targets. The former are a set of bright stars (nominally 300 at m ≤ 8), most of high scientific interest; these are redundantly observed periodically (four times per year) throughout the mission. For the observation of a given target-star (in the reference grid or not), the reference star is chosen from among the approximately 15

Figure 2. Cut-away of the optical bench. The starlight optical path is indicated by dark lines from telescope entry to detectors.

reference-grid stars that lie within the appropriate great-circle band of sky for that target. Each such band has an area of 2159 ≈ 6×360 square degrees (>5% of the sky).

Because of the redundancy of the intra-grid measurements, they can be analyzed to yield a rigid frame;[8] the measurements determine the separations of all pairs of grid stars, even those that could not have been observed simultaneously. Each reference star is thus bright and carefully studied such that it does not significantly slow or corrupt the measurements of non-grid targets. Inter-star angle measurements do not determine overall orientation, so we would observe a few bright quasars redundantly against the grid to provide a link to the best candidate for an inertial frame. (N.B. There are 13 quasars at least as bright as mag 14. Should the quasars show relative motion, there might be significant implications for cosmology or the structure or kinematics of quasars.) With the nominal ±3° articulation range and M=5 (see below), approximately 200 grid stars are needed to provide enough observable pairs for the grid to "lock up;" we envision selecting 300 stars for redundancy and for insurance against the later disqualification of some. Grid stars must be mag 9.5 or brighter to provide high-rate attitude information for pointing stabilization. A 300-star sample grid was constructed using only nearby stars of m ≤ 8. At least 99.9% of the sky had 4 or more reference stars available and 94% of the sky had 10 or more.

The observed grid is largely characterized by a single parameter M, the ratio of the total number of observed pairs to the number of stars. From a series of covariance studies,[11] we find that (a) the mean uncertainty in inter-star angle equals the single-measurement uncertainty for M≈4.2, (b) the uncertainty decreases as ≈M^{-1} in the neighborhood of M=5, approaching $M^{-1/2}$ for M ≈ 15, (c) the uncertainty increases slowly as the number of estimated bias parameters is increased (see below), and (d) the system is robust against deletion of measurements. For a nominal mission of 10 years, quarterly 2 µas observations with M=5 yield, on average, grid star position, parallax, and annual proper motion uncertain by 0.24, 0.16, and 0.08 µas respectively. These results would be a four (4) order of magnitude advance over HIPPARCOS. Note that the 90° nominal angle between two POINTS interferometers results in direct observation of "absolute parallax," yielding a parallax determination two times better than a naive calculation from the coordinate uncertainties in a single series.

In some of the covariance studies, we investigated the determination of instrument bias from the closure information in the astrometric data. In 1981, we found that the form of the bias model is unimportant; the critical parameter is K, the ratio of the number of bias parameters to the number of observations. For K = 0.05 and M = 5, the bias parameter estimation increases the statistical uncertainty in the post-analysis star-position estimate by 7%. This increase with K is approximately linear for K < 0.25. When observations are made in rapid sequence, e.g., every four minutes, this implies 18 bias parameters estimated per day, more than we expect to be necessary. During such times, self calibration from the science data on a time scale of, say, five hours is reasonable. At other times, carefully studied "calibrator pairs" can be revisited several times per day. For an astrometric mission with microarcsecond measurement uncertainty, we consider the ability to extract closure information from the astrometric data an essential feature and the ability to do so quickly, highly desirable.

In the analysis of the data, we would start with the observations of the reference stars and the small set of stabilizing quasars. We would use these data and mild *a priori* estimates of the quasar positions (for alignment with a standard frame) to estimate the five astrometric parameters (two position, two proper motion, and parallax) of each reference star, the positions of the quasars, and a series of instrument model and bias parameters. The resulting stellar coordinate estimates would be both global and bias-free at the level of the uncertainty in the reduced (i.e., combined and analyzed) measurements. Observations of the other targets would then be reduced with the parameters of the reference stars assumed known. Finally, a grand solution would be found in which all data would be analyzed together, without distinguishing the reference-grid stars.

POINTS would nominally operate in perpetual shadow for thermal stability, but the crucial requirement is that sunlight not enter the telescope apertures. A POINTS interferometer could observe a target within 10° of the Sun while the instrument remained entirely shadowed. An excluded zone of 10° radius contains less than 1% of the sky. When one interferometer is targeted near the Sun, the pointing range of the other is restricted. The observable region has been mapped in detail;[12] for a 10° exclusion angle, 91% of all *pairs* are observable on any given day. (Our mission simulations assume a conservative 30° simple exclusion.) A target could be blocked by the Earth or Moon for only a few hours during each four-day orbit; thus Earth and Moon positions add a minor scheduling complication but do not decrease sky coverage.

POINTS would have a rich scientific mission, as indicated by the success of the HIPPARCOS mission[13,14] and the efforts being made within Europe for a follow-on mission, GAIA.[15] Early in its development we discussed the use of

POINTS for planetary system detection,[16] solar-system studies,[8] and astrophysics.[17] The value of microarcsecond astrometry was recognized by the Astronomy and Astrophysics Survey Committee (AASC, a.k.a. Bahcall Committee)[18], which recommended that there be an Astrometric Interferometry Mission (AIM). For recent discussions of astrophysical applications, see Refs. 19 & 20.

3. INSTRUMENT, SPACECRAFT, AND MISSION

The POINTS instrument comprises a pair of independent Michelson stellar interferometers and a laser metrology system that measures both critical starlight paths and the angle between baselines. The primary guiding principle is minimization of systematic error without excess complexity. Critical distances are monitored in real time by laser gauges except for short segments (in the fiducial blocks) that are metered with low expansion material (ULE) in isolated, temperature-regulated enclosures. The spacecraft and mission design[21] provide low thermal disturbance, accurate knowledge of spacecraft velocity in order to correct adequately for stellar aberration, low contamination, continuous access to a large fraction of the sky, and simplified telecommunications. The spacecraft design requires minimal on-orbit deployment.

3.1 Starlight interferometer optics

In each interferometer, the afocal telescopes produce compressed starlight beams, which impinge on the primary beamsplitter (Figure 1). The beamsplitter assembly (PBS, CF, and the spectrometer fold), is mounted on a flexure suspension with PMN actuators to allow correction for OPD variations measured by FAM. In order to obtain broadband throughput and maintain high reliability, all mirrors are overcoated aluminum.* The spectrometer is placed forward to provide a shallow (15°) incidence angle, which makes it easier to design a good (dielectric) beamsplitter for the wide band of interest. This feature also reduces polarization error due to CF, the only unbalanced element preceding the beamsplitter. At the exit ports of the beamsplitter, the light is dispersed and focussed onto a pair of CCD detector arrays.

The primary beamsplitter presents the most difficult coating challenge in the POINTS design. Metallic beamsplitters have substantial loss ($\approx$ 30%). Itek has created a novel multi-layer dielectric design for POINTS.[22,23] There are four requirements, the last three of which would be met exactly in a lossless, mirror-symmetric "sandwich" beamsplitter.[24,23] We anticipate using a beamsplitter that is very nearly lossless and mirror-symmetric. The requirements are: a) $|\mu|$ is small, where $\mu \equiv R - T$, R is the reflectance, and T is the transmittance. Decreasing $|\mu|$ raises fringe visibility and lowers integration time. Currently (in a lossless, non-symmetric design), $\mu = 0.045$ rms. b) $L \equiv 1 - (R + T)$ is small. Currently $L = 1\%$ loss. c) Let ψ be the reflected phase minus the transmitted phase. If ψ varies rapidly with optical frequency, the fringe pattern will be distorted, leading to a loss of sensitivity. In a lossless, symmetric beamsplitter, $\psi = \pi/2$. Currently ψ varies by 450° from 680 to 470 nm. This variation is uncomfortably large, but it can be reduced by re-optimizing the coating, even without symmetry. d) If the "polarization defect," $\Delta^{(b)} \equiv \psi_s - \psi_p$, is non-zero, fringe visibility is degraded and polarized targets show a systematic error. The current design achieves 1.5° rms, which we consider acceptable.

3.2 Spectrometer

The spectrometer[25] is designed to minimize integration time and systematic error. A spectrometer comprises a disperser, imaging system, and detector. A single prism was chosen for the disperser because it has sufficient resolution and higher throughput than a grating. We chose fused silica for the prism because it covers the wavelength range, material of high quality is readily available, and it is readily figured to the required tolerances. For the imaging system, single aspheric mirrors (approximately off-axis paraboloids) yield acceptable geometric aberration. Spectrometer sensitivity has been optimized by varying three parameters: prism wedge angle (29°), mirror focal length (17 cm), and pixel size (20 μm). The integration time is only a weak function of these parameters, which leaves latitude to accommodate secondary requirements, such as Nyquist angle or cross-dispersion resolution. With this spectrometer design, the limiting magnitude is $m_t = 14$, due to sky background light. This limit suffices for ExNPS[26] ($m \leq 10$), and much astrophysics. However, for faint-object astrophysics, a slit could

---

* Silver, which is rarely used on spaceborne mirrors, was considered but rejected because of the possibility of failure due to corrosion before and after launch, and because of the added cost of risk mitigation. For POINTS, with its low reflection count, silver's added throughput does not justify the risk.

be added (requiring two additional mirrors per spectrometer) to yield $m_s = 18$. Note that m_s depends on aperture and is independent of baseline length.

The detectors will have active areas of 256 pixels in the dispersion direction by perhaps 128 across, plus an equal-sized shaded area for readout. Based on presently available technology, we assume that the CCD will have a read noise of 3 e⁻ rms. Cooling to -70°C could keep dark current under 0.002 e⁻/pixel/sec, well below sky background even with a slit. This cooling presents no problem, particularly in high-Earth orbit.

3.3 Astrometric measurement

For the above spectrometer with a nearly lossless beamsplitter, one may calculate the intensity of starlight in each pixel. If δ (the in-plane offset of the target star from the interferometer axis) is estimated by weighted least-squares, then for observing time τ, the measurement standard deviation is

$$\sigma(\delta) = \left(\dot{B}\tau\right)^{-1/2} \tag{1}$$

where $\dot{B}$, the information rate, is[27,28]

$$\dot{B} = \frac{1}{h}\left(\frac{2\pi\ell}{c}\right)^2 \int_{v_-}^{v_+} v\, \bar{G}_n[V,\ s+y]\, I_o(v)\, dv \tag{2}$$

In Eq. (2), ℓ is the baseline length, v_- and v_+ are the passband limits, $I_o(v)$ is the one-telescope detected light intensity, $\bar{G}_n$ is the "information gain" averaged over the fringe, V is the visibility, s is the ratio of stray light to signal light, and y is the ratio of the variance of detector read noise plus dark current to the variance of the signal. The visibility is reduced from unity by reflectance losses of the combining fold, the beamsplitter $\mu \equiv R - T \neq 0$, wavefront error, vibration, pointing variations during one CCD integration, and finite spectrometer resolution. We have[29]

The factor of 2 is a *bona fide* enhancement from making optimal use of the information at the dark fringe. The above three equations are derived in Appendix A. We have done initial work on the estimation[30] from the data of both the stellar position and spectrum. In coordination with us, our colleagues at Moldyn, a subsidiary of Photon Research Associates, have developed and evaluated a suite of fringe estimation algorithms under a NASA SBIR contract.[31]

The limiting magnitude is set by sky background light. To capture most of the starlight and to avoid excessive systematic error from the diffraction-aberration effect[32], it will be necessary to read two of the 256-pixel rows, which corresponds to ≈ 4.8 arcsec on the sky (co-adding the CCD in the cross-dispersion direction before reading, so as to reduce read noise). In the dispersion direction, the 3.6 arcmin acceptance angle for stray light is set by stops on the primaries and the prisms. If a slit is incorporated, the limit in the dispersion direction drops to about that in the cross-dispersion direction, so the limiting magnitude drops to about 18. Starlight throughput is limited by effects detailed in Table II.[33]

For each effect that decreases visibility, we define wavelength-averaged integration-time factors β and γ. (See Table III.) β is the ratio of the integration time with all effects present (i.e., the real instrument) to that with all but the chosen effect present; γ is the ratio of the integration time

Table II. Starlight throughput budget.	
Effect	Factor
Obscuration (fiducial block)	0.82
Primary reflectance	0.84
Diffraction by HOE (1% eff @ 1.06 μm)	0.96
Secondary and 1½ fold mirrors' reflectance	0.69
Beamsplitter absorption	0.99
Reflection losses at beamsplitter (2 surfaces)	0.96
1½ reflections in spectrometer	0.80
Reflection losses at prism (2 surfaces)	0.96
Diffraction (light falls beyond rows of CCD that are read)	0.9
CCD Quantum Efficiency	0.50
Net Throughput	0.15

with only the chosen effect present to that with none present (i.e.. an ideal instrument). An ideal instrument has a 50/50 beamsplitter, no vibration or pointing error, no wavefront error, a spectrometer with infinite resolution, and no detector noise; it rejects all sky background light. Using the extra information near the intensity minima makes integration time a non-linear function of visibility, and $\gamma > \beta$ in each case. Because the various effects that decrease visibility have different dependencies on optical frequency, there is no "net" visibility, and the net integration time factor in Table III is not a product of the β's or of the γ's.

Table III. Integration time (visibility) budget.		
Effect	β	γ
Combining fold, beamsplitter reflectivities	1.011	1.092
Vibration (5 nm rms OPD)	1.005	1.071
Pointing (0.5 mas rms)	1.005	1.069
One-telescope wavefront error = 30 nm rms	1.767	2.137
Spectrometer resolution	1.006	1.059
Detector noise (3 e⁻ rms read noise)	1.001	1.042
Sky background light (m=10 target; no slit)	1.042	1.221
Net integration time w.r.t. ideal instrument (not a product of β's or γ's; see Section VII.C)	2.294	

To make an observation, POINTS must aim both interferometers at targets, damp vibrations, acquire fringes, and accumulate photons while tracking fringes. Slew time is estimated to average 75 sec. Slewing will excite vibrations, especially of the solar array and its boom. These array and boom vibrations will be minimized by tailoring the torque profile; but at some level, POINTS must either track or average over vibrations. The coarse slew would be controlled by the gyros, but should they fail, it could be controlled by counting "extra" reaction-wheel turns. The bright reference star is first brought into the field of view of an instrument-mounted star tracker; the angular velocity must be reduced to $\approx 0.1°$/sec for acquisition by this star tracker. The star-tracker error signal is used to reduce the pointing error to no more than 1.4 arcsec and 0.14 arcsec/sec, which yields 40 fringes on the detector and 2400 photons collected per radian of fringe drift, sufficient for acquisition by the bright-star interferometer. Fast, 20 Hz, measurements of the bright-star fringe provide attitude information for pointing stabilization, which allows long integrations on the fainter targets, limited only by the accumulation of cosmic ray hits on the detector. Integrations of at least five minutes will be possible.

Up to this point, we have assumed that the target stars lie in a great circle containing the two interferometer axes, and that the pseudobaselines (lines joining fiducial points) and baselines (defined via the variation of OPD with instrument rotation) are parallel. Now define the "instrument plane" as containing both pseudobaselines; ζ_i to be the departure of the true baseline i from the corresponding pseudobaseline, projected into the "instrument plane"; ξ_i to be the corresponding departure out of the plane; and δ_i and ε_i to be the in-plane and out-of-plane offsets of target star i. Note that the δ_i are estimated from the starlight fringes, while the ε_i are kept small by the pointing system. The true angle θ between the targets (nearly the angle φ between pseudobaselines) is:

$$\theta = \varphi + (\delta_2 - \delta_1) + E + F \qquad (4)$$

$$E = \zeta_2 - \zeta_1 \qquad (5)$$

$$F = \xi_1 \varepsilon_1 - \xi_2 \varepsilon_2 + \frac{\varepsilon_1 \varepsilon_2 + (\varepsilon_1^2 + \varepsilon_2^2) \cos\varphi}{\sin\varphi} \ . \qquad (6)$$

E is held constant by FAM (with temporal variation too small to be of interest), and its value estimated in the data analysis. The ξ_i and ε_i contributions are non-zero due to manufacturing tolerances, and pointing errors, respectively. The ξ_i and the average values of the ε_i will be under 1 arcsec, and will also be estimated in the data analysis. The ε_i will fluctuate with rms values ≤ 0.2 arcsec and, to the extent that the fluctuations are correlated, the $\varepsilon_1 \varepsilon_2$ term will be non-zero. (NB: $(0.2$ arcsec$)^2$ = 0.2 μas.) The $(\varepsilon_1^2 + \varepsilon_2^2)$ term is suppressed by the factor $\cos\varphi$: $|\cos \varphi| < 0.05$. To obtain this accuracy for ε on faint targets, each interferometer bench has a star tracker that observes several bright stars near the target. To calibrate its direction with respect to the science CCD, the star tracker and the science CCD would observe a single bright star simultaneously. (The above three equations are derived in Ref. 34 and the Appendix of Ref. 11.)

Companions. If the target has a companion separated from it by $\geq$ 2 pixels = 4.8 arcsec in the "transverse direction," i.e., perpendicular to the instrument plane, then the dispersed-fringe spectra will be distinct on the detector and can be analyzed separately. If not, the two positions can be estimated from one distorted dispersed fringe. Even if the target is not known by other means to be a binary, the distortion can in many cases be recognized, in which case the companion(s) can be modelled and the positions determined separately. There will be increased shot noise due to the light of the companion, and the possibility of bias, particularly due to the departures of stellar spectra from blackbody. There is lower error when the target and companion have different temperatures.

If the companion is not modelled and the transverse separation is small, then for small in-plane separations ($\ll \lambda/L$ = 50 mas) the estimator tracks the center of light. For larger in-plane separations, there is an oscillatory bias which, for a companion at least 1 mag fainter, diminishes, with the appropriate filter, to under 1 μas for separations larger than 1 arcsec. Of course, the bias can be removed by correctly modeling the companion(s).

Crowded fields. Some science objectives (e.g., globular cluster studies) require observing in crowded fields. In such fields, light from stars other than the target degrades the measurement of the target. For example, in 47 Tuc, targets within 8 arcmin of the center will suffer substantial increase of integration time if the spectrometer does not have a slit (or within 1 arcmin with a slit). Particularly with a slit, the additional integration time may be partly compensated by estimating simultaneously the positions of other stars that happen to fall in the observable field. We have investigated the ability of POINTS to create an image in a crowded field to obtain the *a priori* target positions needed for astrometric parameter estimation.[35] Although the POINTS baseline length is fixed, we are able to get good "uv-plane" coverage by (1) taking data at several orientations around the direction to the field, and (2) assuming that the field contains unresolved points, so that measurements over the instrument's range of wavelengths yield a radial line in the uv-plane. We considered the target points to have (1) a flat spectrum (test case), and (2) a thermal spectrum (realistic case) which, for the ordinary stars in our study, yields less information far from the uv-plane center.

In the more crowded of the two cases we simulated, there were 18 target points in a field of 2 × 2 arcsec. The closest pair had a separation of 0.025 arcsec (=$\frac{1}{2}(\lambda/L)$, where λ=0.5 μm), should not have been resolved, and differed by 4 mags. With data taken at 15 random orientations of the interferometer, both the flat- and the thermal-spectrum case yielded clear identification of all stars, following deconvolution[36] of the image with CLEAN.[37] The contour plot of the close pair shows the bright star and a large bulge due to the faint star. Data taken with only six random orientations of the interferometer yielded a confusing picture.

A Michelson interferometer is a poor tool for making images. Although it works with small sparse fields, as above, a better procedure is to use a real imager (if available) to study a large field in the region of interest, and then select the astrometric targets. Next, use the interferometer for taking astrometric data that would be reduced by standard methods of parameter estimation. We long ago showed that this procedure would work with POINTS.[38]

Error budget. The instrument error comprises statistical, internal systematic, and external systematic contributions (Table IV). §I. Statistical error is specified as the time required to reach the required accuracy, and has three components, each diminishing as the inverse square root of the integration time. The time required to reach a net uncertainty σ_0 is the sum of the times required for each component individually to reach σ_0. (See Appendix B.) The times given for each component individually are those for determining the offset of a single 8th magnitude star from its interferometer axis to an accuracy of 1.87 μas. The time required to measure both stars is given at the end of §I. Including the net systematic error of 0.68 μas, this integration time yields a total error of 2 μas. §II. Internal error sources (in μas) are the most numerous, and are broken down into instrument systems, and further into effect classes (thermal, misalignment, ...). In our internal documentation,[39] they are further broken down into subsystems and components affected. §III. External error sources are those which would affect an ideal instrument measuring at the same point in space. Intrinsic error sources (e.g., starspots) are treated by Babcock et al.[40]

The error budget is dominated by thermally-driven components; two are particularly large. Their level includes some terms that are upper bounds based on thermal calculations at the current state of the art. When we are able to perform improved calculations, we expect that the error estimates will come down; additionally, we know how to make small design improvements that would significantly reduce these components of the error, if necessary. POINTS will have the benign

thermal environment of high Earth orbit, which it can reach because of its low mass. In some observations, notably in searching for Earth-like planets, the total error must be lower, ≈0.3 µas. To achieve this, the statistical error will be reduced by observing bright stars and making a large number of repeat measurements. However, the 0.68 µas systematic error of Table IV appears too large. Fortunately, some of the error components are expected to average down over a number of observations, and some we expect to remove by modelling.

Table IV. POINTS error budget summary.	
I. Statistical error (integration time for 8th magnitude target star)	Time
Photon statistics (ideal instrument), one star	28 sec
Non-ideal telescopes/spectrometer, one star	34 sec
Suboptimal fringe estimator, one star	2 sec
Net integration time, two 8th magnitude stars	128 sec
II. Internal systematic error.	$\sigma(\theta)$[a]
Metrology[10]	
Thermal: direct effects, dn/dT or warp of an element[b]	0.37 µas
Misalignments, including thermal effects on structure	0.21
Articulation-angle-dependent: defects in modelling, e.g., in beamwalk map	0.00
Unmodelled fiducial block rotation	0.36
Polarization	0.03
Diffraction	0.01
Laser frequency drift	0.00
Laser gauge systematic error	0.19
Telescopes and Beamsplitter	
Thermal: direct effects, dn/dT or warp of an element[b]	0.00
Polarization	0.15
Phase vs. Optical Frequency	0
Vibration third moment	0.04
Beamwalk	0.00
Wavefront error third moment	0.00
Spectrometer	
Input beam shifts/tilts[25,41]	0
Spectrometer element tilts/rotations	0.02
Temperature change	0.05
Diffraction/aberration	0.16
Polarization	0.15
III. External systematic error.	
Ephemeris[42]	0.17
Geometry[34] (also in App. A of Ref. 11)	0.05
Net systematic error, §§II and III combined (i.e., RSS)	0.68 µas
[a] Entries of "0.00" in this column indicate that the calculated value is zero to the accuracy shown. Entries of "0" indicate that a full calculation is not yet available, but that based on preliminary calculations, we expect that the error in question can be made insignificant. [b] dn/dT, where n is refractive index and T is temperature.	

3.4 Optical bench

The optical bench (Figure 2) is fashioned from graphite-cyanate sheets of (2D) low thermal expansion, and comprises top and bottom plates connected by peripheral and radial walls and the central cylindrical hub. The hub provides a mounting ring for the articulation flexure. The two telescopes are separate units; each telescope can be aligned internally before being joined to the optical bench at three points, which provide for simple final alignment. A recent analysis of the vibration modes of a single optical bench, fully loaded with optics, showed no eigenfrequency below 100 Hz.

Within each telescope, a light-weighted primary mirror is mounted by three flexures, each constraining two degrees of freedom but soft in the other four degrees; the set of three locates the mirror without transferring stress to it, as in the ARPA-sponsored Teal Ruby telescope.[43,44] See Figure 3. At the front of the telescope tube, the fiducial block's container (a double-wall shield) and the secondary are held in place by separate three-leg spiders. As shown in Figure 4, the fiducial block is suspended within its container by six stingers (flexure-hinged rods that ideally transmit only axial force and no torque) in three pairs. At each connection to the fiducial block, the stingers join an Invar disk bonded to the fiducial block via a glass pedestal,[45] which filters thermal stresses induced by the Invar disk. The spiders in the two sides must be in the same orientation, *not mirror images,* in order that the images overlap when the beams are combined. The aperture is defined at the primary by a mask, so that the starlight and FAM light will see the same aperture.
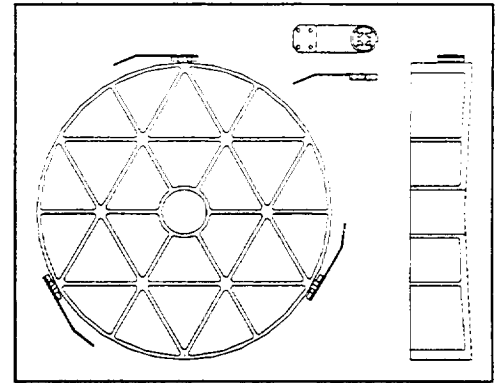

Figure 3. A light-weighted primary mirror and its support suspension, in plan and cross section.

3.5 Laser gauges

The POINTS starlight optics are surveyed into position by a set of laser interferometric distance gauges; this scheme employs Michelson interferometry to stabilize the starlight OPD within each interferometer to within a few picometers, and cornercube resonators to measure the angle between the two interferometers to within a few picoradians. This alignment and measurement is done with the aid of fiducial points, each defined by the apices of a cluster of four cornercube retroreflectors (retros), which are mutually coincident within a micron. Each such cluster is part of a fiducial block. The fiducial block was conceived in 1980[46] in terms of its required function. As its detailed design has been refined, it has also become more clearly manufacturable.[47,48]

The two fiducial points in each interferometer define a pseudobaseline; the angle φ between pseudobaselines is determined from measurements of the six distances linking the four fiducial points. The starlight OPD is referred to the pseudobaseline by measurements of the FAM OPD (from the auxiliary beamsplitter to the primary beamsplitter via the holographic optical elements, or HOEs, on the primary mirrors) and an auxiliary OPD (from the auxiliary beamsplitter to two retros in the fiducial blocks and back). The difference of distances from each "athermal lens" to the corresponding primary must be held constant, to within ~70 pm.[1] (The athermal lens, used to spread the FAM light over the primary, is mounted on the fiducial block and is separated from the fiducial point by about two cm of ULE glass in a
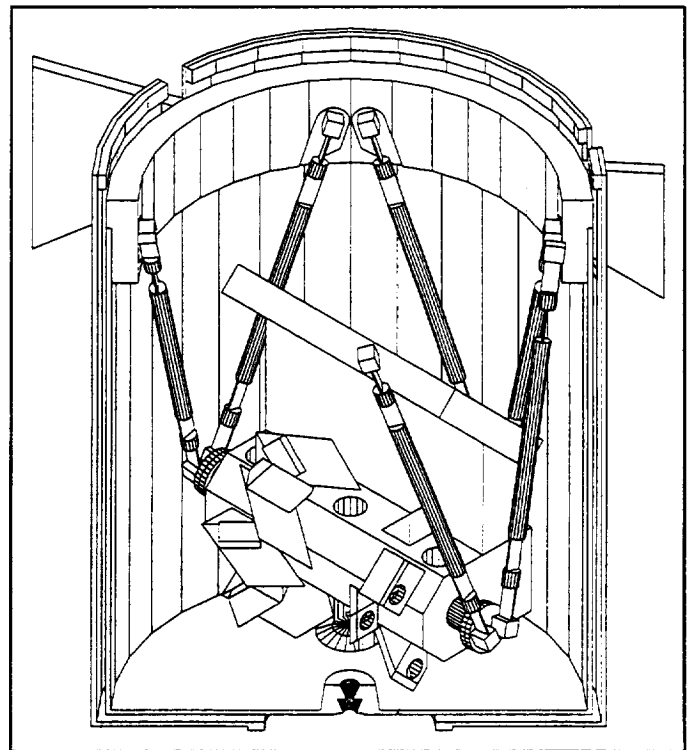

Figure 4. The fiducial block is suspended by six stingers from its support ring (at the top of the can), which is held by a three leg spider; two legs are shown.

thermally stable environment.) For holding this distance, we use the "focus gauge," which measures the OPD from the auxiliary beamsplitter to a pair of retros mounted on the primary mirrors. In conjunction with the auxiliary gauge and its servo, the focus gauge produces an error signal when there is a change in the OPD from the fiducial points to their respective primaries. In response to this error, PMN actuators, operated differentially, move each fiducial block's spider with respec: to the telescope tube.

The angle φ is measured with six resonant cavities made from the 12 remaining retros in the fiducial blocks. In each cavity, we plan to use two independent gauging systems with counter-propagating beams (at slightly different optical frequencies) for redundancy. The 6° articulation range requires the resonant gauges to have a 3° range in the laser incidence angle. Cornercube (retro) endpoints permit this range, and show no error under a uniform thermal expansion of the glass. A resonator has several advantages over the Michelson approach here: absence of glass in the optical path, larger displacement sensitivity, and lower sensitivity to injected-beam misalignment. Also, using one curved mirror among the six in each cavity (common in two-mirror cavities) loosens the assembly tolerances and improves operation.

The resonant gauge output is periodic in the apex-apex length L (with period $\lambda/2$) and in the laser frequency ν (with period = free spectral range (FSR) = c/2L). The Michelson interferometer outputs are also periodic in OPD (with period λ) and laser frequency (FSR = c/OPD). To sense deviations of the length or OPD, we use frequency modulation and phase-sensitive detection; a servo keeps the amplitude modulation at zero either by repositioning an optic (Michelson gauges) or by shifting the laser frequency to track the distance change (resonant gauges). In the latter approach, the frequency shift is very nearly proportional to the displacement.

3.6 Alignment

In the FAM system, the laser metrology wavefronts are superposed on the starlight wavefronts by the HOEs on each primary mirror. The most critical alignments govern this superposition; the most severe tolerances for a 1 pm error contribution are on the HOE-to-athermal-lens spacing, 70 pm, and on tilt of the primary mirror, 4 nrad. For the spacing, the focus gauges were added. For the tilt, a simple (quad-cell) alignment system is all that is needed. Each requirement is far less severe than those on FAM and the determination of φ. Most tolerances for a 1 pm error contribution are in the range 0.1-1 µrad and 0.05-1 µm. Some alignments are held by servos, and some are adequate passively.

Much of the basis for the alignment procedures is contained in a pair of SPIE papers by Noecker et al. (1) "Internal Laser Metrology for POINTS"[1] discusses our laser gauges, their laboratory development and testing, the optical design and characteristics of the point-to-point gauges that use retroreflector cavities, the beam injection and extraction for them, and the servo techniques for keeping the injected beams aligned over the 6° of baseline articulation. (2) "Optic-Misalignment Tolerances for the POINTS Interferometers"[10] addresses the effects on the OPD both for starlight and for laser light of 21 displacements or rotations of components or assemblies that, based on preliminary calculations, seemed most important.[*] Phillips[47] describes and gives algorithms for the alignment during manufacture of the set of four retroreflectors in the fiducial blocks.

3.7 Fine pointing and isolation system

The actuator for the Fine Pointing and Isolation System (FPIS) is a hexapod, or Stewart platform. FPIS accepts a blended and transformed signal from the bright-star interferometer (in-plane pointing), the star trackers on each interferometer's optical bench (out-of-plane pointing), and accelerometers at the bus end of the FPIS struts (active vibration isolation); it holds the in-plane pointing stable to ~0.5 milliarcsec (mas) and out-of-plane pointing stable to ~0.1 arcsec rms. Either interferometer may serve as the designated bright-star interferometer for a particular observation. By looking at a star of mag < 9.5, the bright-star interferometer provides in-plane pointing estimates with 0.2 mas resolution every 50 msec. The on-instrument star

---

[*] Noecker's lowest-order analytic expressions and Murison's numerical raytracing results were carefully cross-checked. The most significant discrepancies in the displacement and rotation tolerances were less than a few percent. Murison also produced four computer-symbolic-algebra raytracing results, which agreed with tolerances from his numerical ray-trace to 5 significant figures.
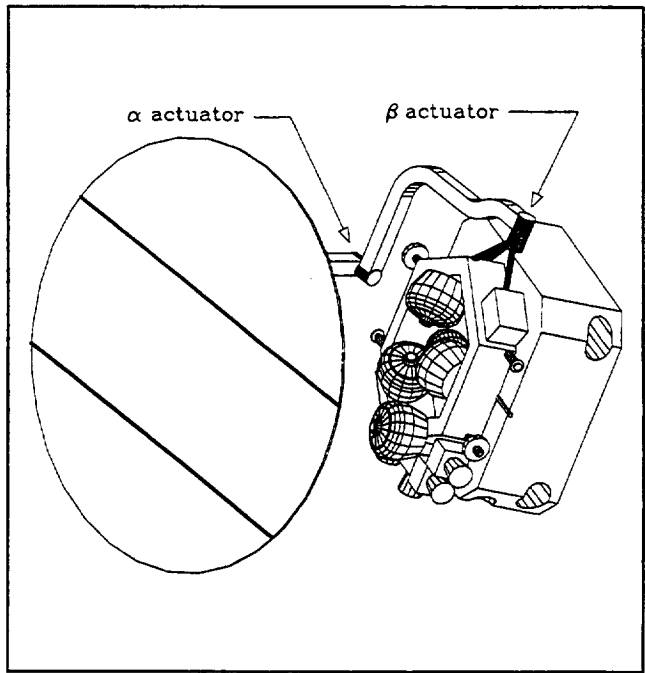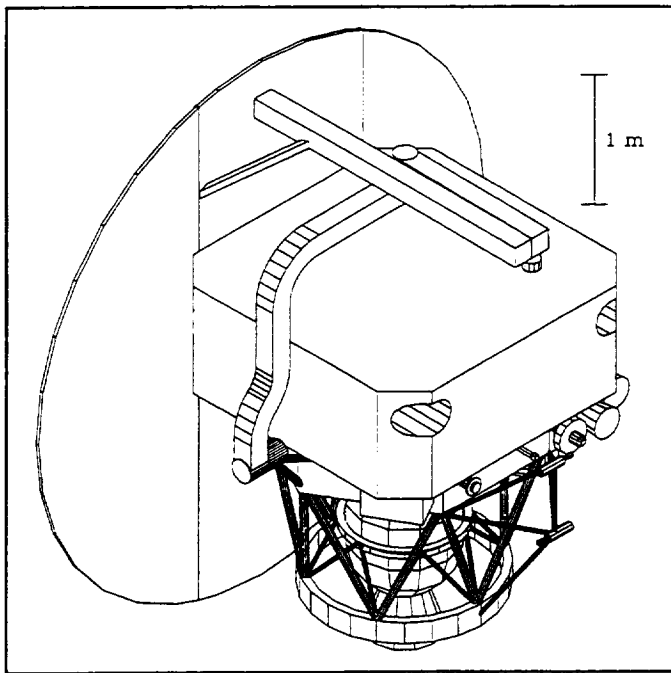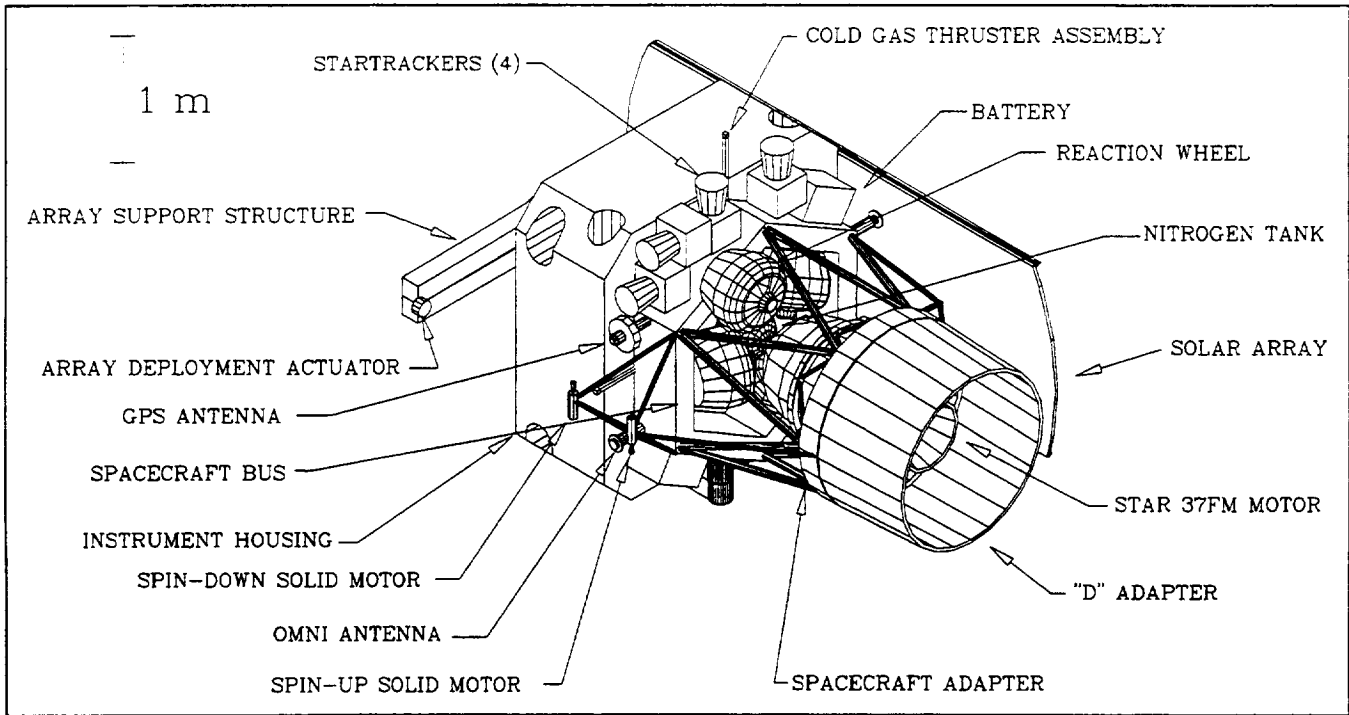
Figure 5. The spacecraft in three configurations: top, launch; left, cruise; and right, operation. (D. Noon, JPL)

trackers in each stellar interferometer provide out-of-plane pointing estimates rapidly, with 0.1 arcsec resolution. (These can be provided advantageously, and at 0.3 sec intervals, by an interferometric star tracker we have devised, with 2.5 cm apertures and a 6 cm baseline. It is a derivative of the Newcomb[49] interferometer.)

FPIS connects three evenly spaced points on a ring on the spacecraft bus with another triplet on one of the interferometers. The lengths of all 6 legs of the hexapod are adjustable magnetically or with PMN or PZT actuators; by adjusting the appropriate combination, one may adjust the interferometers in any of the 6 rigid-body degrees of freedom. (The two interferometers are connected by the articulation mechanism.) Such hexapods are under development at JPL, Harris, and TRW.3.8 Thermal analysis and control

3.8 Thermal analysis and control

POINTS thermal control is layered, with modest demands at each layer: solar shield (to shade the instrument during operation), instrument enclosure (with active wall regulation to 0.5 K and baffled telescope ports), optical bench and telescope tubes, and enclosures for small devices. Because of the self calibration discussed in Section 2.2, long-term (i.e., > 5 hours) temperature control is not required in any part of the instrument. Some of the small devices require that average ("soak") temperature and maximum point-to-point difference be constant to 1 mK each over a 5 hr period. For example, the fiducal blocks are enclosed in double-wall aluminum cans, and never see a change in point-to-point difference greater than 10^{-4}K. The laser reference cavity requires 0.1 K regulation, an easy improvement over the 0.5 K regulation of its immediate environment.

A series of thermal analyses (using TRASYS and SINDA-G) were performed at Itek.[50] These addressed the equilibrium temperature distribution for the instrument pointing toward and parallel to the solar shield, which was assumed to be uninsulated and thus hot. From these studies, we conclude that the required temperature and temperature gradient stabilities are comfortably met by the present design, without addition of shield insulation or consideration of the beneficial effects of the long thermal time constants in the instrument.

3.9 Orbit

Our preference for a low-disturbance, low-contamination, thermally quiet environment, access to a maximal amount of sky, and a long mission life are best satisfied with a heliocentric orbit or a high Earth orbit. The long mission life and ease of telecommunications favor the latter. A high Earth orbit constrains the instrument mass more than a low orbit, and it poses different challenges for spacecraft angular-momentum management (since it is outside Earth's magnetic field, preventing the use of magnetic torque devices, but it is subject to a much reduced gravity-gradient torque from Earth), for telemetry, and for orbit determination. Since the flight-system design summarized here meets each of these challenges with generous margin, a high Earth orbit has been baselined. Anywhere above about 60,000 km offers excellent access to sky, short solar occultation times, and avoidance of Earth's radiation belts. Anywhere below about 150,000 km can be handled easily by the systems baselined for telemetry and orbit determination. The nominal choice is a circular orbit with 100,000-km radius and 27° inclination to Earth's equator (consistent with a Florida launch), which yields an orbital period of about 3.6 days. The combination of an Atlas IIAS launch vehicle with a Centaur upper stage and a Star 37FM (Thiokol) solid-fuel rocket motor for orbit circularization is capable of delivering a payload of about 1750 kg to the nominal orbit. This is a generous match for the POINTS payload, which is estimated to be about 1350 kg (i.e., 30% margin). See Schumaker, et al.[21] for a discussion of several aspects of delivery to orbit.

An orbit determination study[42] was based on a small GPS-like beacon[51] on the spacecraft and a modest observing schedule using six autonomous GPS receivers. In the less optimistic of the two cases investigated, 12 two-hour observation sequences were spaced over four days (approximately one spacecraft orbital period). During a 15 day period centered on the observing sequences, the spacecraft velocity uncertainty remained under 0.25 mm/s, the limit in the error budget; during a 10 day period, 0.15 mm/s; and during the four days of observing, 0.09 mm/s. Thus, the error-budget limit could be met comfortably with a reasonable observing schedule.

4. CONCLUSION

POINTS was conceived as an instrument to test general relativity to second order by measuring the deflection of starlight by the Sun. This goal was abandoned when it became apparent that the required (≈100 m) boom for an occulting disk would be prohibitive. By that time, other goals had come to the fore. These included astrophysics[17] and the search for remote planets. For at least the last decade, the central thrusts have been to understand and reduce both systematic error and total

mission cost. These goals imply an instrument that is simple and small. However, large size enhances precision *via* baseline length and photon statistics.

On retrospect, we identify four key architectural decisions. 1) The instrument would be pointed at selected targets, and not an all-sky survey device (e.g., HIPPARCOS). A pointed instrument better addresses the science goals, in part because of the need for very high measurement accuracy. 2) Access to a large field in which to find a reference star after the target star had been chosen would be by changing the angle between two independent stellar interferometers and by rotating the instrument around the target direction. An alternative approach involving adjustable delay lines and siderostats was rejected because of cost, complexity, reliability and its implications for mission life, and possible increase in mechanisms for systematic error. 3) The angle between the two baselines would be about 90 deg. (We believe that one to two radians is fine.) This maximizes both the field available for finding a reference star and the ability to determine absolute parallax. A large inter-baseline angle supports rapid closure on the sky and thus self calibration. 4) The fringe would be detected as a channelled spectrum. Forming the fringe spatially with a large optical passband lowers the visibility and (especially if visibility is otherwise high) lowers the information rate. The dispersed fringe can be detected far off axis, which simplifies the initial finding of the fringe. Finally, by preserving the full dispersed fringe (or an archival version that is independent of offset, δ), it is possible to reanalyze the data to include information about target structure (e.g., a binary). While this is possible with a spatially formed fringe, astrometric efficiency requires observing exclusively the central fringe, where the visibility is high.

The above decisions and the selected small size led to the design of an instrument with four key attributes. 1) There are a small number of optical elements altogether, and importantly before the beamsplitter. 2) The optical bench is stiff, with the minimum eigenfrequency found computationally to be above 100 Hz when the bench is loaded with optics. 3) The instrument could be placed in high Earth orbit without excess cost. 4) The low mass and mass moments permit quick slews. Historically, low mass and size have correlated with low cost. Although the instrument requires no new invention, some of the technologies are new, and would require development and certification for space. Based on cost studies at Itek and TRW (which excluded cost reductions possible with *anticipated* technologies), POINTS could be flown within the $250M estimate for AIM in the report of the Astronomy and Astrophysics Survey Committee (AASC, *a.k.a.* Bahcall Committee)[52]

5. APPENDIX A: ESTIMATOR

An interferometer that detects the intensity of combined beams as a function of optical frequency using dispersion, path difference using dithering, or other modulating parameter, has a *fringe visibility* defined as

$$V = \frac{I_{max} - I_{min}}{I_{max} + I_{min}} \tag{7}$$

where I_{max} and I_{min} are the maximum and minimum intensity over one period of the fringe pattern as a function of the modulation parameter. When $V=1$, the sensitivity is greatest; when $V=0$, the sensitivity is zero. In this Appendix, we derive the information rate for $V<1$, independent of the causes of the visibility reduction. A more complete treatment is available elsewhere.[29]

Astrometric interferometers such as POINTS, in which the visibility is very near 1 and in which a dispersed fringe *(channelled spectrum)* is employed, can take advantage of a non-obvious enhancement in sensitivity. Integration time may be reduced as much as a factor of two. Heuristically, in the portions of the fringe near the minima the derivative of signal with respect to OPD is high, but the signal is small, so the shot noise is low. This causes the information rate to rise sharply near unit visibility. Visibility in POINTS is limited to ~0.85 by wavefront error. The improvement in information rate is a factor of ~1.3.

The combined effect of reductions of visibility, noise, and background can be summed up as τ/τ_{id}, the ratio of the actual integration time to that of a corresponding "ideal" interferometer. τ/τ_{id} is inversely proportional to the information rate $\dot{B}$. $\dot{B}$ is proportional to the *information gain, G*.

Detected intensity. We will first calculate the detected intensity as a function of optical frequency ν and angular offset of the star δ. Suppose that the star is a point source, and creates equal detectable spectral intensities I_o in each telescope. (I_o is power per unit optical frequency times detector quantum efficiency.) The phase difference is

$$\beta = \frac{2\pi\delta\ell v}{c} \quad . \tag{8}$$

where ℓ is the baseline, 2 m. The detectable spectral intensity, on sides of the beamsplitter denoted '+' and '-', is

$$I_\pm = I_o \left(1 \mp V' \sin\beta \right) \tag{9}$$

where V' is the visibility, ignoring the reduction due to spectrometer resolution and pixel size.

Detector effects and sky background. We now calculate the number of counts in a detector cell covering an optical frequency range $(v_i - \Delta v, v_i + \Delta v)$, averaged over one CCD integration time τ, taking detector noise and sky background into account. Let the number of electrons resulting from the readout process in a particular pixel be $\tilde{N}_{read}$, which we assume to have a Gaussian distribution with zero mean. Let the rms of $\tilde{N}_{read}$ over time be N_{read}. Let $\dot{N}_{dark}$ be the rate of detection of dark current electrons (e.g., thermally-generated ones) in a pixel.

The sky surrounding the target contributes background light of spectral intensity S_v from an area of 4.8 arcsec by 3.6 arcmin without a spectrometer slit, or by ~5 arcsec with a slit. The corresponding sky brightnesses are magnitude 14.2 and 18.3. We define

$$s \stackrel{d}{=} \frac{S_v}{I_o} \quad . \tag{10}$$

We assume that the sky background and the star both have the spectrum of a 5777 K blackbody.

Integration over resolution element. Thus the number of photoelectrons in filter pixel i (centered at frequency v_i) after an integration of duration τ is

$$N_{i\pm} = \tau \int_{v_i - \Delta v}^{v_i - \Delta v} \frac{I_o}{hv_i} \left(1 + s \mp V' \sin\beta \right) dv + \tilde{N}_{read} + \tau\dot{N}_{dark} \quad . \tag{11}$$

Neglecting the v-dependence over one pixel of all quantities in (11) except $\sin\beta$, this is

$$N_{i\pm} = N_i \left\{ (1 + s) \mp \chi V' \sin\beta \right\} + \tilde{N}_{read} + \tau\dot{N}_{dark} \tag{12}$$

where

$$N_i \stackrel{d}{=} \frac{2\Delta v \tau I_o}{hv_i} \quad , \quad \chi = \text{sinc}\,\Delta\beta \stackrel{d}{=} \frac{\sin\Delta\beta}{\Delta\beta} \quad , \quad \Delta\beta \stackrel{d}{=} \frac{2\pi\delta\ell\Delta v}{c} \quad . \tag{13}$$

Astrometric uncertainty. We next find $\sigma(\delta)$, including the above effects and starlight shot noise.

$$\sigma(\delta) = \frac{1}{\sqrt{B}} \tag{14}$$

where $B = B_+ + B_-$ is the inverse covariance matrix (which is 1×1), and

$$B_\pm = \sum_i \left(\frac{\partial N_{i\pm}}{\partial\delta} \right)^2 \left[\sigma(N_{i\pm}) \right]^{-2} \quad . \tag{15}$$

Information in an integration of duration τ. In taking the derivative in (15), we may neglect the derivative of χ, which involves $\sin \Delta\beta$, since the derivative of $\sin \beta$ is larger by a factor $v/\Delta v$. We have

$$\frac{\partial N_{i\pm}}{\partial \delta} \simeq \mp \frac{2\pi \ell v_i}{c} N_i V \cos\beta , \quad V \stackrel{d}{=} \chi V' .$$ (16)

For the starlight and dark current, Poisson processes, the variance of a number M of detected carriers is M. The rms of the read noise is N_{read}, so its variance is N_{read}^2. Thus,

$$\left[\sigma(N_{i\pm})\right]^2 = N_i \left\{(1 + s + y) \mp V \sin\beta\right\} , \quad y \stackrel{d}{=} \frac{N_{read}^2 + \tau \dot{N}_{dark}}{N_i} .$$ (17)

Substituting into (15), we have

$$B_\pm \simeq \sum_i \frac{\left(\frac{2\pi \ell v_i}{c}\right)^2 N_i V^2 \cos^2\beta}{(1 + s + y) \mp V \sin\beta} .$$ (18)

Combining B_+ and B_-,

$$B \simeq 2\sum_i \frac{(1 + s + y)\left(\frac{2\pi \ell v}{c}\right)^2 N_i V^2 \cos^2\beta}{(1 + s + y)^2 - V^2 \sin^2\beta} .$$ (19)

Putting back in the definition of N_i, and converting from a sum to an integral (recall that N_0 is the number of detected photons in the optical frequency interval $2\Delta v$, so that $2\Delta v \to dv$)

$$B \simeq \left(\frac{2\pi \ell}{c}\right)^2 \frac{\tau}{h} \int_{v_-}^{v_+} v\, I_0(v)\, \bar{G}_n(V, \beta, s + y)\, dv$$ (20)

where

$$\bar{G}_n(V, \beta, s + y) \stackrel{d}{=} \frac{2(1 + s + y) V^2 \cos^2\beta}{(1 + s + y)^2 - V^2 \sin^2\beta} .$$ (21)

Integration over one fringe. We will simplify (20) by averaging over one cycle of β, i.e. over one fringe. We will ignore the variation over the cycle of β of all quantities except $\sin\beta$ and $\cos\beta$. (Recall that the interferometer will be operated approximately 5 fringes away from boresight on the star, so this approximation is adequate but not extremely accurate.) It can be shown[53] that

$$\bar{G}_n(V, s + y) \stackrel{d}{=} \frac{1}{2\pi} \int_{-\pi}^{\pi} d\beta\, \bar{G}_n(V, \beta, s + y) = 2(1 + s + y)\left[1 - \sqrt{1 - \left(\frac{V}{1 + s + y}\right)^2}\right] .$$ (22)

$\bar{G}_n(V, s + y)$ is used in place of $\bar{G}_n(V, \beta, s + y)$ in evaluating (20). It is also possible to treat (20) with the more drastic assumption that the visibility is independent of wavelength[54]. This allows an analytic solution for integration time[25].

Results, analysis, and summary. Since the various effects on visibility depend differently on wavelength, the visibility cannot be separated into a product of visibilities attributable to individual causes, except at a particular optical frequency. The best that can be done is, for each effect, to define wavelength-averaged integration-time factors β (the improvement from the real instrument that its absence would yield) and γ (the degradation from the ideal that its presence would cause). An ideal

instrument has a 50/50 beamsplitter, no vibration or pointing error, no wavefront error, a spectrometer with infinite resolution, and no detector noise, and rejects all sky background light. Because the various effects that decrease visibility have different dependencies on optical frequency, there is no "net" visibility. As functions of optical frequency, one may define visibilities attributable to individual causes, and a net visibility. These quantities are less useful for making design decisions than the β and γ defined here, which are simple numbers.

In the low-noise, high-visibility case, (22) has the expansion

$$\bar{G}_n(V, s+y) = 2\left\{1 - \sqrt{2(v+s+y)} + (s+y)\right\} \tag{23}$$

where $v \overset{d}{=} 1 - V$. In leading order, detector noise and sky background have the same effect as a reduction of visibility, but in the next order, they are different: visibility does not appear. In the high-noise case,

$$\bar{G}_n(V, s+y) = \frac{V^2}{1+s+y} \quad , \tag{24}$$

which has been shown to be the same as the result obtained with a suboptimal estimator in which the photon counts at the + and - ports are differenced, then processed[28].

6. APPENDIX B: SUM OF TIMES

In many cases of interest, we wish to know the measurement time required to reduce the uncertainty of the estimate $\hat{x}$ of a quantity x to a given level σ_o, where x is the sum of quantities v_i (i=1,...,n). We obtain a convenient result when the measurements of v_i are mutually uncorrelated random variables with white noise, and thus $\hat{x}$ is a random variable with white noise of variance

$$\sigma_x^2 = \sum_{i=1}^{n} \sigma_i^2 \tag{25}$$

where σ_i^2 is the variance of v_i. If T_i is the time required for measuring v_i such that σ_i is equal to σ_o, then

$$\sigma_x^2 = \sum_{i=1}^{n} \frac{\sigma_o^2 T_i}{T} \quad . \tag{26}$$

where all v_i are measured for a time T. Then we have $\sigma_x = \sigma_o$ when

$$T = \sum_{i=1}^{n} T_i \tag{27}$$

A similar result holds when x is the product of v_i. In this case, T_i is the time required to measure v_i to a fractional precision $\sigma_i / v_i = \sigma_o / x$.

7. ACKNOWLEDGMENTS

8. REFERENCES AND NOTES

SAO/PAG Technical Memoranda are available from R.D. Reasenberg, reasenberg@cfa.harvard.edu, 617-495-7108.

1. M.C. Noecker, J.D. Phillips, R.W. Babcock, and R.D. Reasenberg, "Internal laser metrology for POINTS," in *Spaceborne Interferometry*, R.D. Reasenberg, ed., Proc. SPIE **1947**, pp. 174-187, 1993.
2. The Smithsonian Institution holds a patent for a "System for Measuring Distance Between two Points using a Variable Frequency Source," number 5,412,474, dated 2 May 1995. It covers both the incremental distance measurements

needed for POINTS and tested in the laboratory and absolute gauging, which we would demonstrate in the laboratory based on a natural extension of the previous laboratory work, were it shown to be needed.

3. Y. Gürsel, "Laser metrology gauges for OSI," in *Spaceborne Interferometry*, R.D. Reasenberg, ed., Proc. SPIE **1947**, pp. 188-197, 1993.

4. N.M. Sampas and D.Z. Anderson, "Stabilization of laser beam alignment to an optical resonator by heterodyne detection of off-axis modes," *Appl. Opt.* **29**, 3, pp. 394-403, Jan 1990; N.M. Sampas and D.Z. Anderson, private communications (1984-92).

5. R.W. Babcock, TM91-10: "POINTS and the Traveling Salesman Problem," SAO/PAG Technical Memorandum, 21 Oct 1991.

6. R.D. Reasenberg and I.I. Shapiro, "An optical interferometer in Earth orbit for testing general relativity," in *Space Relativity -- Acta Astronautica*, **9**, (Proceedings of the 5th International Symposium on Space Relativity, Dubrovnik, Oct. 78), W. Wrigley, ed. pp. 103-106, 1982.

7. M.L. Agronin, "Precision actuators for spaceborne interferometers: a tutorial," in *Spaceborne Interferometry*, R.D. Reasenberg, ed., Proc. SPIE **1947**, pp. 140-160, 1993. Each flexure pivot has three blades. The redundancy permits tensioning the blades, which reduces the torsional stiffness around the rotation axis without softening the other five degrees of freedom.

8. R.D. Reasenberg, "Microarcsecond astrometric interferometry," in *Proceedings of the Workshop on High Angular Resolution Optical Interferometry From Space*, P.B. Boyce and R.D. Reasenberg, eds. BAAS, **16** (3,II), pp. 758-766, 1984.

9. R.D. Reasenberg, "Microarcsecond astrometric interferometry," in *Astrometric Techniques, Proceedings of IAU Symposium # 109*, H.K. Eichhorn and R.J. Leacock, eds., pp. 321-330, 1986.

10. M.C. Noecker, M.A. Murison, and R.D. Reasenberg, "Optic-misalignment tolerances for the POINTS interferometers," in *Spaceborne Interferometry*, R.D. Reasenberg, ed., Proc. SPIE **1947**, pp. 218-233, 1993.

11. R.D. Reasenberg, R.W. Babcock, M.C. Noecker, and J.D. Phillips, "POINTS: The first small step," in *Spaceborne Interferometry*, R.D. Reasenberg, ed., Proc. SPIE **1947**, pp. 12-29, 1993.

12. R.W. Babcock, TM94-01: "Sky Visibility Revisited," SAO/PAG Technical Memorandum, 26 Jan 1994.

13. J. Kovalevsky, "The need for very accurate optical astrometry by interferometric techniques," in *Proceedings of the ESA Colloquium on Targets for Space-based Interferometry*, ESA **SP-345**, pp. 9-11, 1992.

14. Astron. and Astrop., **258**, pp. 1-141, Springer International, 1992. See 21 papers in section "Celestial Mechanics and Astrometry."

15. L. Lindegren, M.A.C. Perryman, U. Bastian, J.C. Dainty, E. Høg, F. van Leeuwen, J. Kovalevsky, A. Labeyrie, S. Loiseau, F. Mignard, J.E. Noordam, R.S. Le Poole, P. Thejil, and F. Vakill, "GAIA: global astrometric interferometer for astrophysics," in *Amplitude and Intensity Spatial Interferometry II*, J.B. Breckinridge, ed., Proc. SPIE **2200**, pp. 18-26, 1994.

16. R.D. Reasenberg and I.I. Shapiro, "POINTS the planet finder," BAAS, **11**, p. 554, 1979.

17. R.D. Reasenberg, R.W. Babcock, J.F. Chandler, M.V. Gorenstein, J.P. Huchra, M.R. Pearlman, I.I. Shapiro, R.S. Taylor, P. Bender, A. Buffington, B. Carney, J.A. Hughes, K.J. Johnston, B.F. Jones, and L.E. Matson, "Microarcsecond optical astrometry: an instrument and its astrophysical applications," Astron. J., **96**, 1731-1745, 1988.

18. *The Decade of Discovery in Astronomy and Astrophysics*, National Research Council, National Academy Press, Washington, DC, 1991.

19. S.T. Ridgway, "The scientific support for a space interferometry mission," in *Spaceborne Interferometry*, R.D. Reasenberg, ed., Proc. SPIE **1947**, pp. 2-11, 1993.

20. D.M. Peterson, "Scientific support for interferometry from space," in *Spaceborne Interferometry II*, R.D. Reasenberg, ed., Proc SPIE **2477**, pp. 2-8, 1995.

21. B.L. Schumaker, J.S. Ulvestad, M. Agronin, G.-S. Chen, W.D. Ledeboer, J.W. Melody, D.E. Noon, C.-Y. P. Peng, "POINTS Spacecraft Studies, 1992-1994 Progress Report," Technical Report, Jet Propulsion Laboratory, Pasadena, CA, 30 June 1994.

22. J.D. Phillips, TM94-13: "Itek beamsplitter: calculated performance," SAO/PAG Technical Memorandum, 11 Aug 1994.

23. J.D. Phillips and C. Hickey, "Beamsplitters for astronomical optical interferometry," in *Spaceborne Interferometry II*, R.D. Reasenberg, ed., Proc. SPIE **2744**, pp. 132-148, 1995.

24. J.D. Phillips, TM94-12: "Beamsplitter constraints," SAO/PAG Technical Memorandum, 11 Aug 1994.

25. J.D. Phillips, "A spectrometer for astronomical interferometry," in *Spaceborne Interferometry II*, R. D. Reasenberg, ed. Proc. SPIE **2477**, pp. 149-163, 1995. §9 discusses beam shifts and tilts.

26. ExNPS is the NASA program for the Exploration of Neighboring Planetary Systems; it is part of "Origins."

27. R.W. Babcock, TM92-05: "POINTS Astrometric Sensitivity," SAO/PAG Technical Memorandum, 21 September 1992.

28. R.D. Reasenberg, TM85-01: "Astrometric Precision," SAO/PAG Technical Memorandum, 11 March 1985.

29. J.D. Phillips, TM96-xx: "POINTS Sensitivity," SAO/PAG Technical Memorandum, in preparation, 1996.

30. R.D. Reasenberg, "Kalman-Filter Fringe Tracking in an Optical Interferometer," in *Amplitude and Intensity Spatial Interferometry*, J.B. Breckinridge, ed., Proc. SPIE **1237**, pp. 172-182, 1990.

31. C.E. Padilla, H.M. Chun, L. Matson, and R.D. Reasenberg, "Fringe tracking filters for space-based interferometers," in *Spaceborne Interferometry*, R.D. Reasenberg, ed., Proc. SPIE **1947**, pp. 30-43, 1993.

32. M.C. Noecker, "Systematic errors in high-precision optical interferometric astrometry" in *Spaceborne Interferometry I*, R.D. Reasenberg, ed., Proc. SPIE **2744**, pp. 188-208, 1995.

33. Reflectance, reflection loss, and absorption estimates are from calculations at Itek by C. Hickey and W. Davis.

34. R.D. Reasenberg, TM92-09: "The POINTS measurement of a star-pair separation: the effect of both the offset of the target from the corresponding instrument axis and the rotation and skew of the interferometer baseline," SAO/PAG Technical Memorandum, 15 December 1992.

35. The study was performed by Lincoln Greenhill of CfA. The results were presented by Reasenberg to the Space Interferometry Science Working Group on 1 June 1995.

36. T. Cornwell and R. Braun, "Deconvolution," in *Synthesis Imaging in Radio Astronomy*, R.A. Perley, F.R. Schwab, and A.H. Bridle, eds., Astronomical Society of the Pacific Conference Series, **6**, pp. 167-183, 1989.

37. F.R. Schwab, "Relaxing the isoplanatism assumption in self-calibration; applications to low-frequency radio interferometry," *Astron. J.*, **89**, pp. 1076-1081, 1984.

38. R.W. Babcock and R.D. Reasenberg, TM86-4: "The effect on POINTS of a dim companion to a target star," SAO/PAG Technical Memorandum, 6 March 1986; Babcock's unpublished notes.

39. J.D. Phillips, TM96-xx: "POINTS Error Budget," SAO/PAG Technical Memorandum, in preparation, 1996.

40. R.W. Babcock, J.D. Phillips, and R.D. Reasenberg, "An astrometric planet search, POINTS simulations and mission characteristics," in preparation, 1996.

41. J.D. Phillips, TM93-09: "Error Due to Position Shifts in the Spectrometer," SAO/PAG Technical Memorandum, 7 Oct 1993.

42. B. Haines and S. Lichten, "POINTS orbit determination with GPS-like beacon," JPL Interoffice Memorandum 335.8-92-036, Dec. 8, 1992. (Also in Schumaker *et al.*, 1994, *op cit.*)

43. J.W. Pepi and R.J. Wollensak, "Ultra-lightweight fused silica mirrors for a cryogenic space optical system," in *Space Optics*, C.L. Wyman, ed., Proc. SPIE **183**, pp. 131-137, 1979.

44. J.W. Pepi, M.A. Kahan, W.H. Barnes, R.J. Zielinski, "Teal Ruby — design, manufacture and test," in *Optics in Adverse Environments*, M.A. Kahan, ed., Proc. SPIE **216**, pp. 160-173, 1980.

45. B.L. Schumaker, M. Agronin, G-S. Chen, W. Ledeboer, J. Melody, D. Noon, and J. Ulvestad, "Spacecraft and mission design for the Precision Optical INTerferometer in Space (POINTS)," in *Spaceborne Interferometry*, R.D. Reasenberg, ed., Proc. SPIE **1947**, pp. 58-72, 1993.

46. R.D. Reasenberg, TM80-07: "POINTS design concept: the fiducial block," SAO/PAG Technical Memorandum, 15 Aug 1980.

47. J.D. Phillips, TM95-02: "POINTS Fiducial Block Adjustment and Assembly Procedure" SAO/PAG Technical Memorandum, 25 Jan 1995.

48. J.D. Phillips, TM96-xx: "Fiducial block manufacturing plan," SAO/PAG Technical Memorandum, in preparation, 1996.

49. R.D. Reasenberg, R.W. Babcock, J.D. Phillips, K.J. Johnston, and R.S. Simon, "Newcomb, a scientific interferometry mission at low cost," in *Amplitude and Intensity Spatial Interferometry II*, J.B. Breckinridge, ed., proc SPIE **2200**, pp. 18-26, 1994.

50. Neither the software (TRASYS is single precision) nor the algorithms themselves give the precision needed in the POINTS thermal analysis. The results presented should be considered preliminary.

51. C. Dunn and L. Young, "POINTS navigation beacon straw man design," JPL Interoffice Memorandum 335.9.003-93, Jan. 29, 1993. (Also in Schumaker *et al.*, 1994, *op cit.*)

52. *The Decade of Discovery in Astronomy and Astrophysics*, National Research Council, National Academy Press, Washington, DC, 1991.

53. I.S. Gradshteyn and I.M. Ryzhik, "Table of Integrals, Series, and Products," Academic Press, NY, 4th ed., p. 379, eq. 3.647, 1965.

54. J.D. Phillips, TM94-07: "Newcomb Limiting Magnitudes," SAO/PAG Technical Memorandum, 10 May 1994.